CO_2/Brine/Carbonate Rock Interactions: Dissolution and Precipitation

Poster presented at the Fourth Annual Conference on Carbon Capture & Sequestration, Alexandria, Virginia, May 2-5, 2005

Reid B. Grigg & Robert K. Svec, New Mexico Petroleum Recovery Research Center; Peter C. Lichtner & William Carey, Los Alamos National Laboratories; and Charles E. Lesher, University of California, Davis

INTRODUCTION

Determining the viability, risks, and optimal locations of sequestering carbon dioxide (CO_2) in the subsurface requires detailed knowledge of the complex interactions among CO_2, rock matrix, and pore fluids under reservoir pressure and temperature. Many physical and chemical processes are known to occur both during and after geologic CO_2 injection, including diagenetic chemical reactions and associated permeability changes. Together with hydrated CO_2, cations from brines may form solid-state carbonate minerals, ostensibly providing permanent sequestration.

Reported here are findings and comparison of five large coreflooding experimental series preformed on quarried and reservoir carbonates (limestone and dolomite) with co-injected or alternating injections of CO_2 and brine at reservoir conditions. Metal chlorides were added as tracer components in injection brines for three tests and appeared in quantities well above natural levels in deposited carbonates in one test. Core segment porosity and permeability are reported to indicate dissolution and deposition. Cores were sectioned and analyzed by chemical and back-scattered electron imaging (BSEI) and chemical titration for compositional changes. In two tests fluid samples taken at reservoir conditions and neutron computed tomography (CT) were used to monitor changes in in-situ fluid compositions and the development of the 3-D porosity structure of the flooded cores, respectively.

Dissolution of carbonates at reservoir conditions during co-injection of CO_2 and brine was confirmed by porosity and permeability increases, neutron CT, and brine compositional analysis performed on effluent brine samples obtained at reservoir conditions. When deposition occurred it was indicated by porosity and permeability reductions in down stream core, BSEI identification, and modeling. The composition and extent of deposits was strongly influenced by the brine composition. Deposition and dissolution were found to occur in close proximity. The results are being used to calibrate a CO_2 model coupling multiphase flow to chemical reactions that will be used to predict in situ dissolution and deposition related to CO_2 geologic sequestration.

Table 1.
Brine compositions used in the series of five large corefloods.

	Reservoir Brine #1	Reservoir Brine #2	Brine #3 Tracer #1	Brine #4 Tracer #2
NaCl	64700	13531	10000	25000
$CaCl_2$	11000	4330	5000	4040
$MgCl_2$	3810	1914	5000	190
$NaHCO_3$	1850	5645		
Na_2SO_4	5590	4831		
$MnCl_2$			5000	198
$SrCl_2$			5000	
TDS	86950	30251	30000	29428

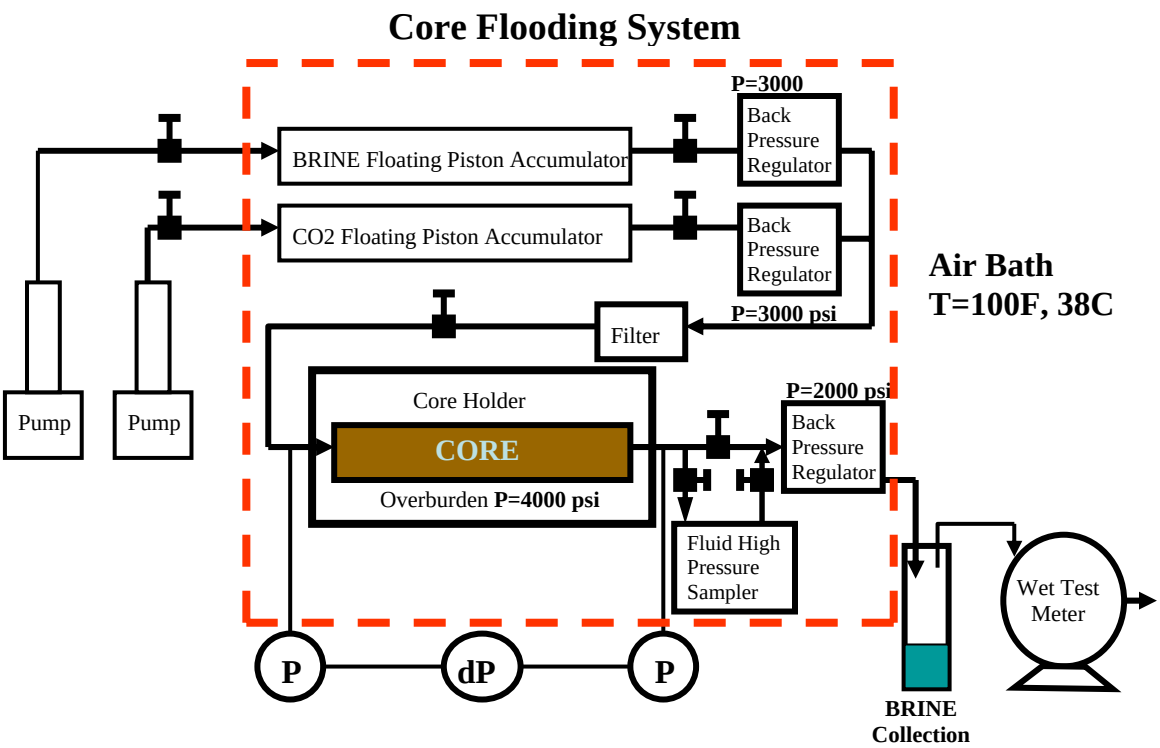

Figure 1. The coreflooding apparatus is set up for alternate or co-injection of two fluids. The effluent can be sampled under ambient or system (installed for last two experiments) conditions.

COREFLOOD A – INDIANA LIMESTONE

The first coreflood was on quarried Indiana limestone at 2000 psig and 100ºF using Reservoir Brine #1 (Table 1). Brine was injected alternating with CO_2 (WAG). After injecting several hundred pore volumes a 25 cm long solution channel had formed while the permeability of the whole core was essentially the same as the fresh core (Figures 2 and 4). There was no evidence of plugging though the second half of the core had a permeability reduction of about ½ which is an indication of deposition (Figure 3). Using BSEI and compositional analyses all possible deposition had the same composition as the fresh core, thus in Coreflood C metal tracers were added to aid in identifying deposition.

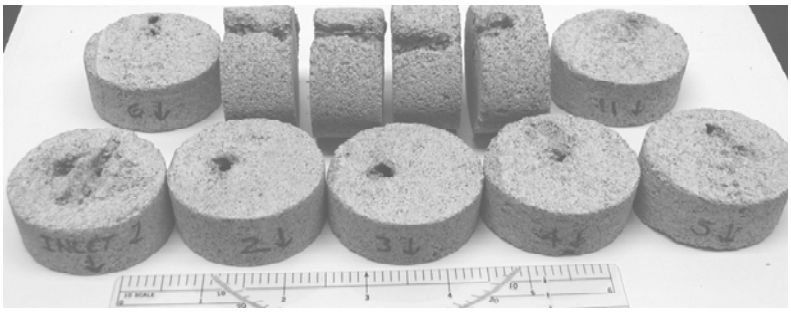

Figure 2. Post-WAG Indiana limestone dissolution channel extends from inlet face into first half of core length (~ 25 cm).

Figure 3. Second half of the core did not have a solution channel (last ~ 25 cm). Final permeability of unchannelled core, k=19.5 mD. Initial perm in this same region before WAG ~ 36 mD.

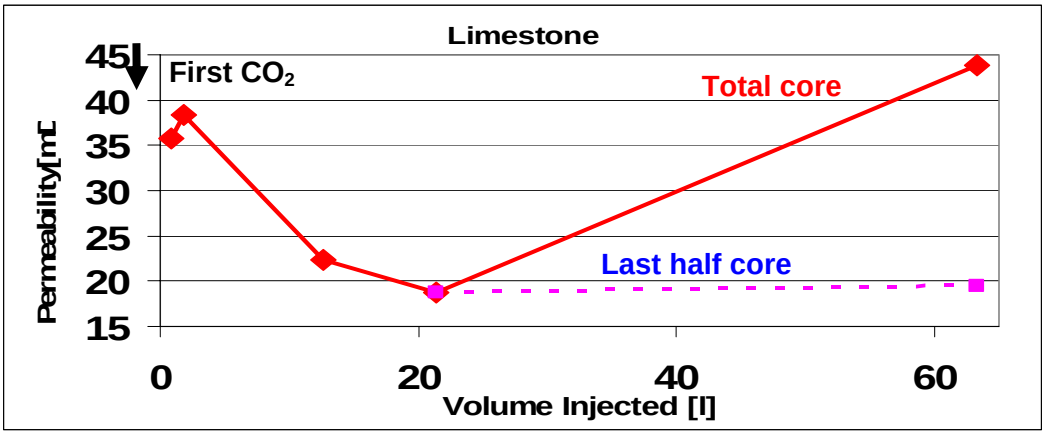

Figure 4. Limestone Permeabilities

Coreflood B – San Andres Dolomite

The second coreflood was on San Andres core from the Seminole field in west Texas (Figure 5). The primary component of the San Andres is dolomite. A significant increase in porosity occurred during the brine flood (Figure 6) due to anhydrite dissolution. Brine #2 composition was patterned after Seminole produced water (Table 1). Extensive porosity and permeability increases occurred during the WAG portion of the flood with dissolution of dolomite and further dissolution of anhydrites (Figures 7 and 8)**.**

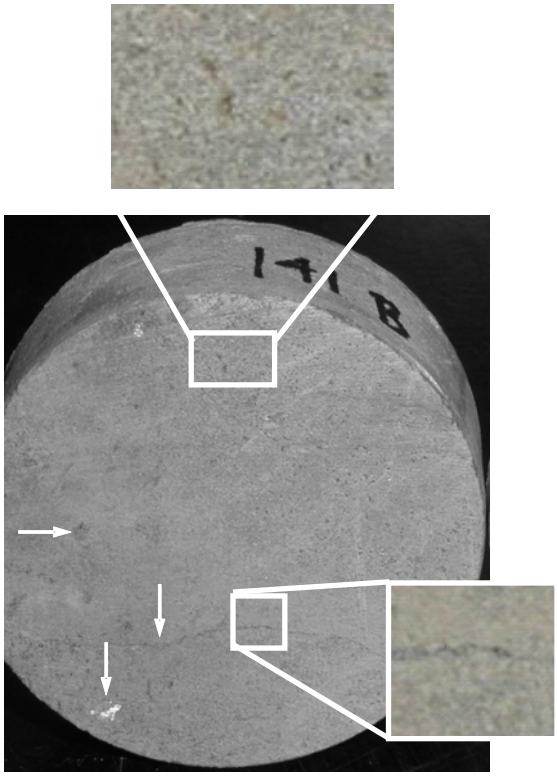

Figure 5. Pre-flood dolomite, Seminole San Andres, Gaines county TX. Vuggy anhydritic very fine grain dominated packstone, anhydrite nodules, and stylolites.

Figure 6. Post waterflood sectioned core after brine flood showing anhydrite dissolution.

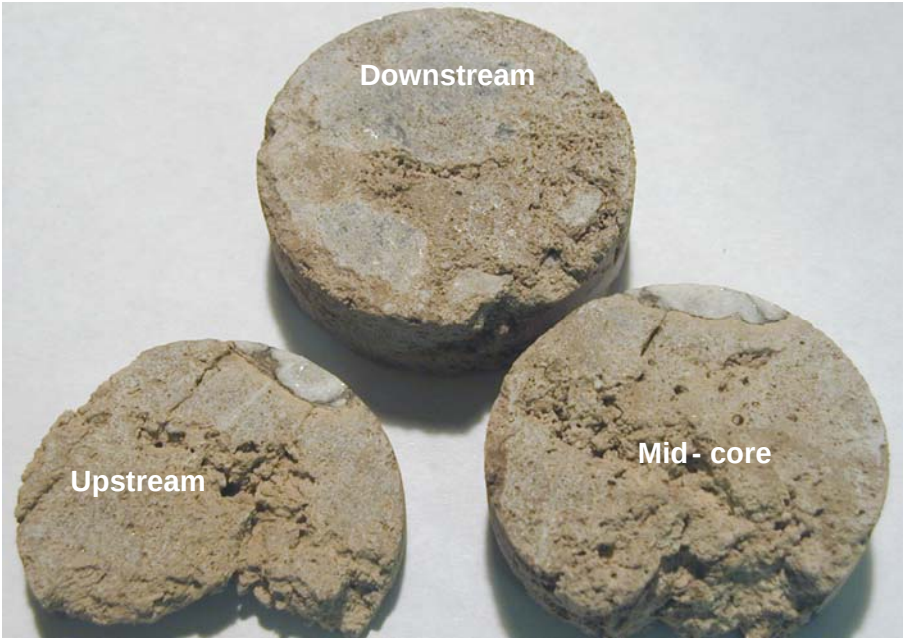

Figure 7. Post-WAG Seminole San Andres core showing dolomite dissolution with additional anhydrite dissolution

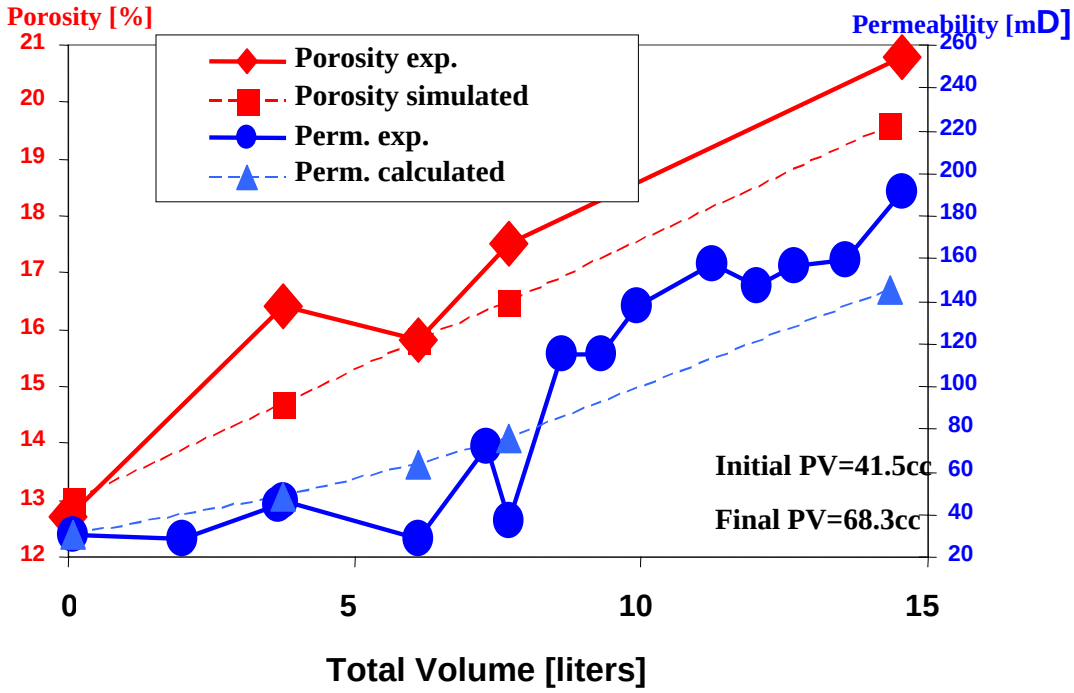

Figure 8. Measured and calculated porosity and perm during the flooding of San Andres dolomite.

COREFLOOD C – INDIANA LIMESTONE WITH BRINE #3 TRACER #1

The third coreflood was on quarried Indiana limestone core (Figure 9) with a co-injection of brine with high levels of metal tracers Manganese and Strontium added to the brine as chlorides which are naturally found at very low levels in this limestone. The limestone is over 98% calcite (Figures 14 and 15) in the non-reacted areas. A solution channel formed in the first 15 cm of Segment A (Figures 10 and 11). Significant deposits of manganese and strontium occurred as carbonates throughout the core (Figures 13-15) shown in the plot above and BSE images and quantitative analysis shown below. It was suspected that the system was over saturated with the tracer carbonates and that in a new system the tracer quantities would be reduced significantly.

	Diameter [cm]	Length [cm]	Porosity [%]
Segment A	5.03	17.15	16.91
Segment B	5.03	39.37	17.54
Entire Core	5.03	56.52	17.35

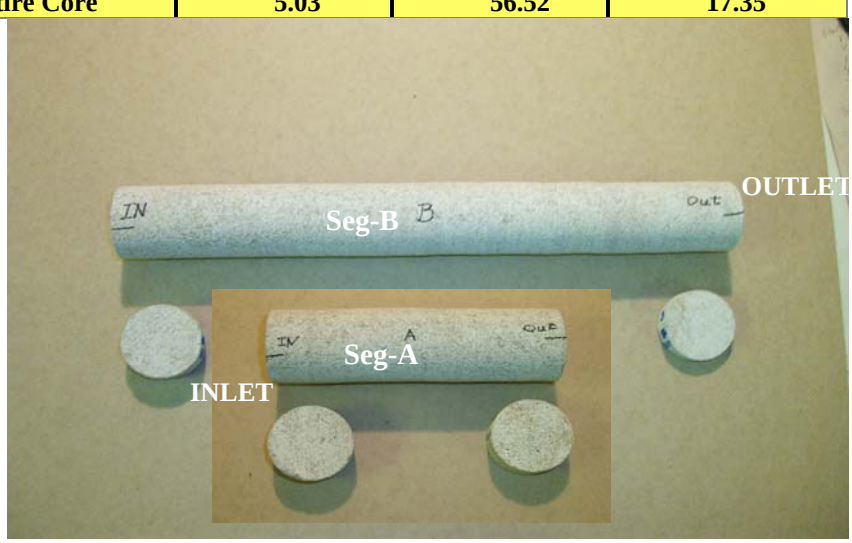

Figure 9. Pre-flood limestone core.

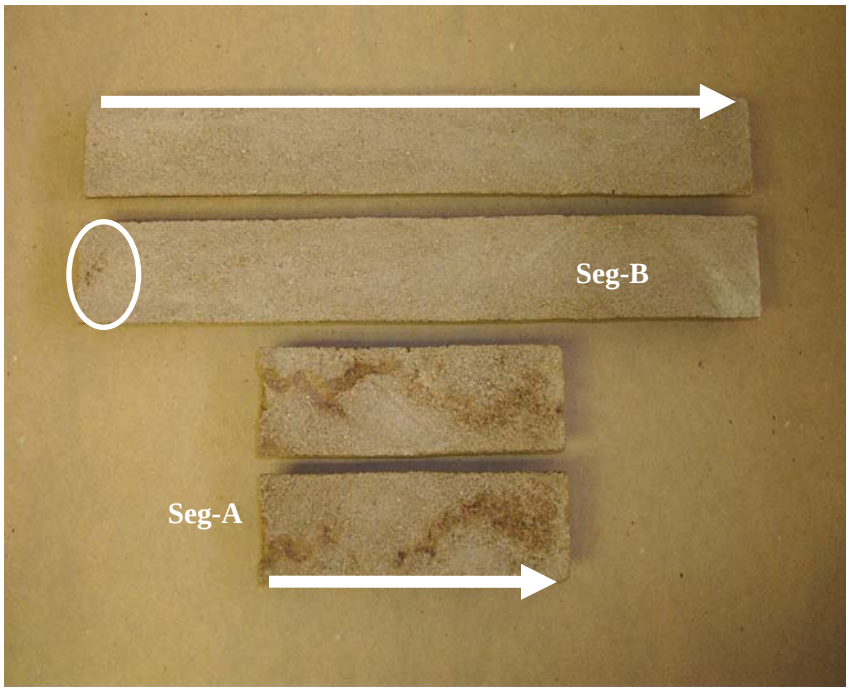

Figure 10. Post-flood limestone core sectioned.

Figure 11. End view of Segment A inlet.

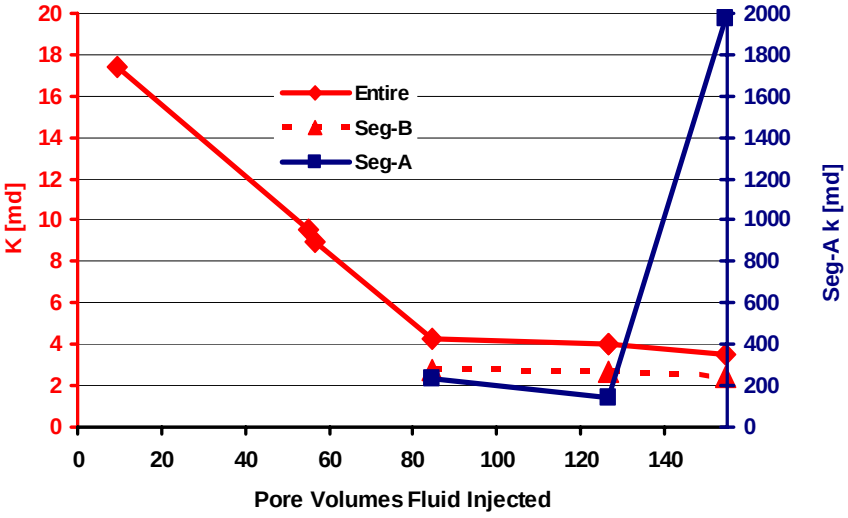

Figure 12. Permeability results limestone (Coreflood C).

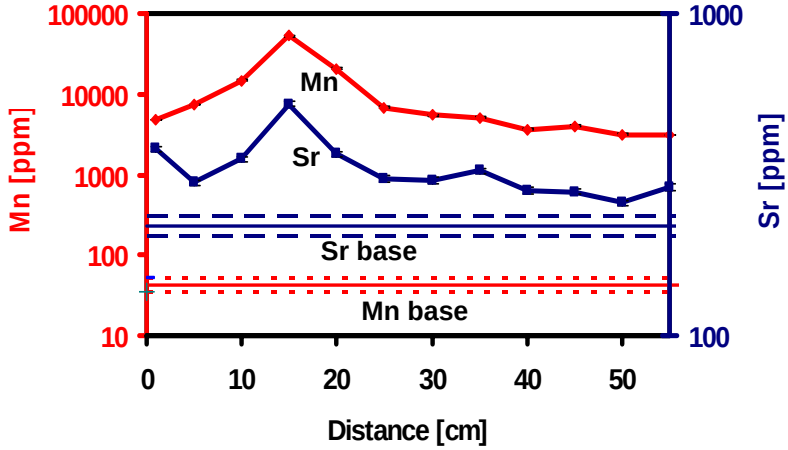

Figure 13. Cross section composition for Manganese and Strontium along the length of the both core segments in Coreflood C.

	Ca	Mg	Mn	Sr
1.	98.7	0.65	0.62	0.00
2.	35.2	0.32	64.1	0.20
3.	19.4	0.30	79.7	0.28

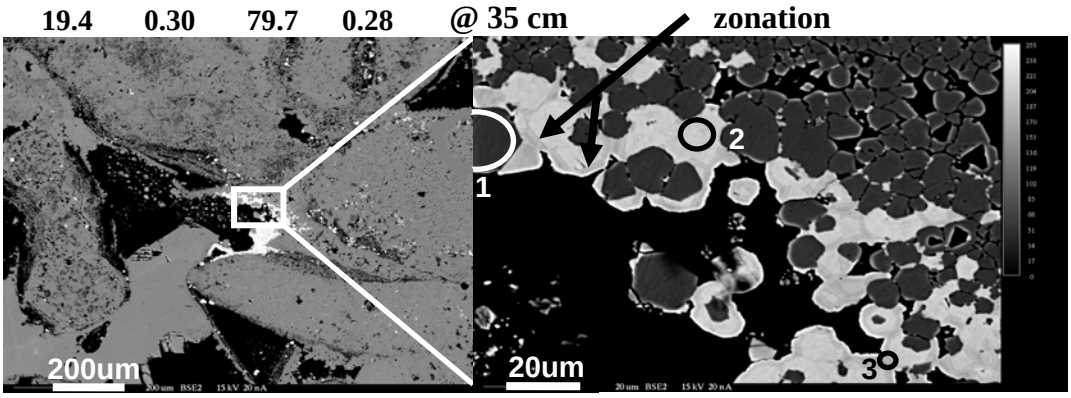

Figure 14. BSE Quantitative analysis [% as carbonate] for Calcium, Magnesium, Manganese, and Strontium.

	Ca	Mg	Mn	Sr
1.	98.9	0.94	0.05	0.00
2.	30.5	0.47	68.6	0.26

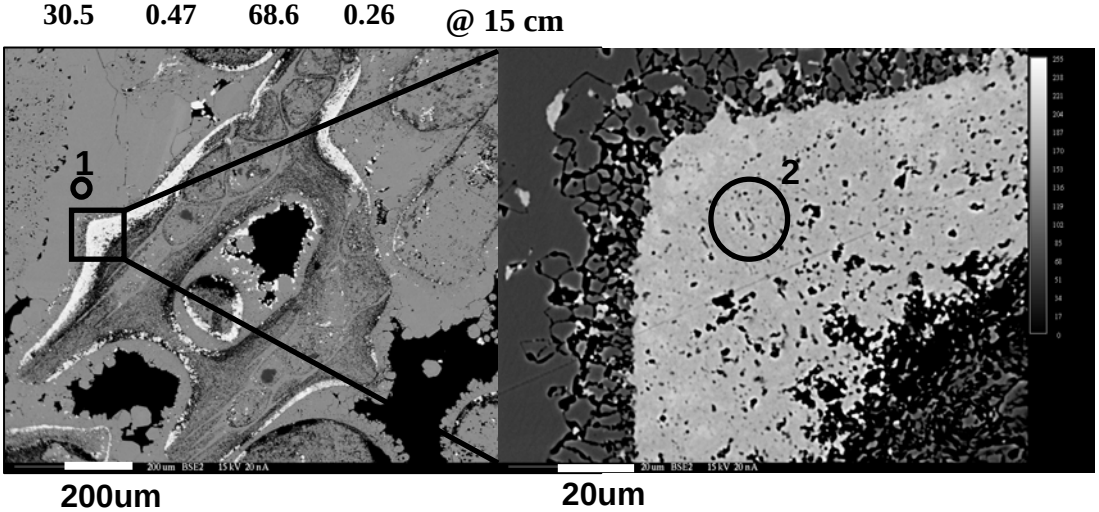

Figure 15. BSE Quantitative analysis [% as carbonate] for Calcium, Magnesium, Manganese, and Strontium.

COREFLOOD D – INDIANA LIMESTONE & COREFLOOD E – LOCKPORT DOLOMITE (both with Brine #4 Tracer #2)

The fourth (D) coreflood was on quarried Indiana limestone. The fifth (E) coreflood was on quarried Lockport dolomite. Each was performed at 2000 psig and 100ºF with co-injected CO2 and Brine #4. Brine #4 compared to Brine #3 contained no strontium, less than 4% as much manganese and magnesium, similar calcium concentration, and increased sodium to make up to a similar level of dissolved solids. The intent was to have levels of tracer high enough to detect but not high enough to saturate the system with manganese. In addition to the tests performed during the earlier test series three CT scans were performed on each core segment: one on the fresh core, one at an interval during the flood, and the final after the last flood period; a bromide tracer diffusivity test for each system (Figures 20-23 and 29-32), and in situ fluid samples taken for compositional analysis to compare with ambient samples.

Figure 16 is a view of all three limestone sections after the first flood period. The flood had to be stopped because the core sleeve failed due to dissolution creating a cavity near the inlet. In the limestone test injection was interrupted twice due to sleeve failure. After each flood period the core was trimmed. Figure 17 compares the ends after the three flooding periods. Figures 18 and 19 are color enhanced CT images on the fresh core (I), after the first flooding period (II), and following the last flooding period (III) as a cross section at about 6 cm deep (Figure 18) and 90º longitudinal sections (Figure 19) for each of the three times with the location of the cross section indicated. Figures 20-23 are plots of produced compositions taken during the diffusivity test for limestone. Figure 20 shows the produced bromide concentration versus pore volumes injected. The first part is with the bromide spiked Brine #4 displacing unspiked Brine #4. The later stage is a displacement with a coinjection of CO2 and Brine #4. CO3 as calcite in solution is also plotted showing an increase of dissolved carbonate with the presence of CO2. Figures 24-32 are similar figures for dolomite.

In each system there was an increase in porosity and permeability for the three core segments (Figure 28). Most of the increase was in the first core segment, but there were small increases in porosity and permeability in the two downstream segments. There was not sufficient data in the limestone for a definitive value, but the dolomite had 14% porosity increase in Segment A and 0.8 and 0.4% porosity increases in Segments B and C, respectively, or a system increase of 5% (9.9 cm3). The mass loss calculated using effluent compositions is over 23 g or over 8.0 cm3. Neither BSEI or chemical analysis detected any tracer precipitation in either core type.

Some observations in comparing the limestone and dolomite results are:

1. Comparing Figure 20 with 29, it is noted that the flow behavior of the limestone indicates a less homogeneous flow distribution than that of dolomite.
2. Figures 21 and 30 compare the production of manganese that in both cases has a reduction after a soaking period early in the test. There is a spike in produced manganese concentration corresponding to CO2 breakthrough. There appears to be some manganese precipitation in the early time in the core that is produced after CO2 breakthrough. At ambient conditions most of the manganese precipitates.
3. Figures 22 and 31 compares the effluent calcium concentrations. In both systems solution calcium increases after CO2 breakthrough with significant concentrations precipitating at ambient conditions. The higher concentration of calcium is in the limestone that has little magnesium in the solution.
4. Figures 23 and 32 compare magnesium concentration in the effluent. There was little change in either system until CO2 breakthrough. As might be expected the increase in effluent concentration is small in limestone (~30%) which contains less than 1% magnesium while increases about eight fold in dolomite which contains about equal mole concentrations of magnesium and calcium. Most of the magnesium stays in solution at ambient conditions with little precipitation in either system.

In summary there was no precipitation detected in Corefloods D and E. The primary difference that was noted with earlier floods was a significant change in brine composition. Each of the first three brines (including the reservoir brines) had much high levels of magnesium and the first tracer brine had high levels of manganese and strontium.

Figure 16. Three limestone core segments after the first flooding period.

Figure 17. First segment inlet after each flooding period (limestone Coreflood D).

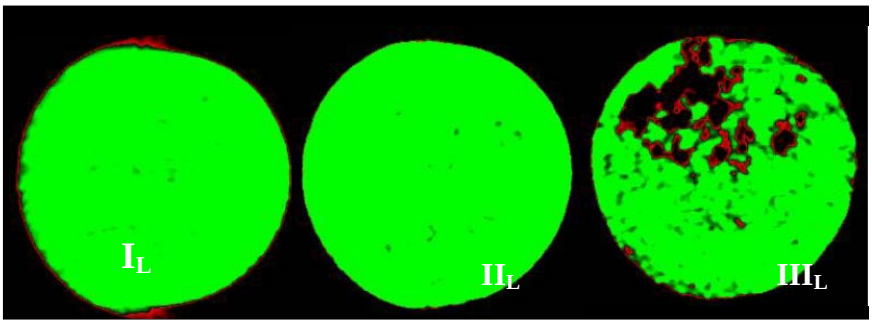

Figure 18. CT cross section images at ~6 cm from the end of the original limestone Segment A inlet. Pre-flood (I_L), after the first flooding period (II_L), and post-flood (III_L) (limestone Coreflood D).

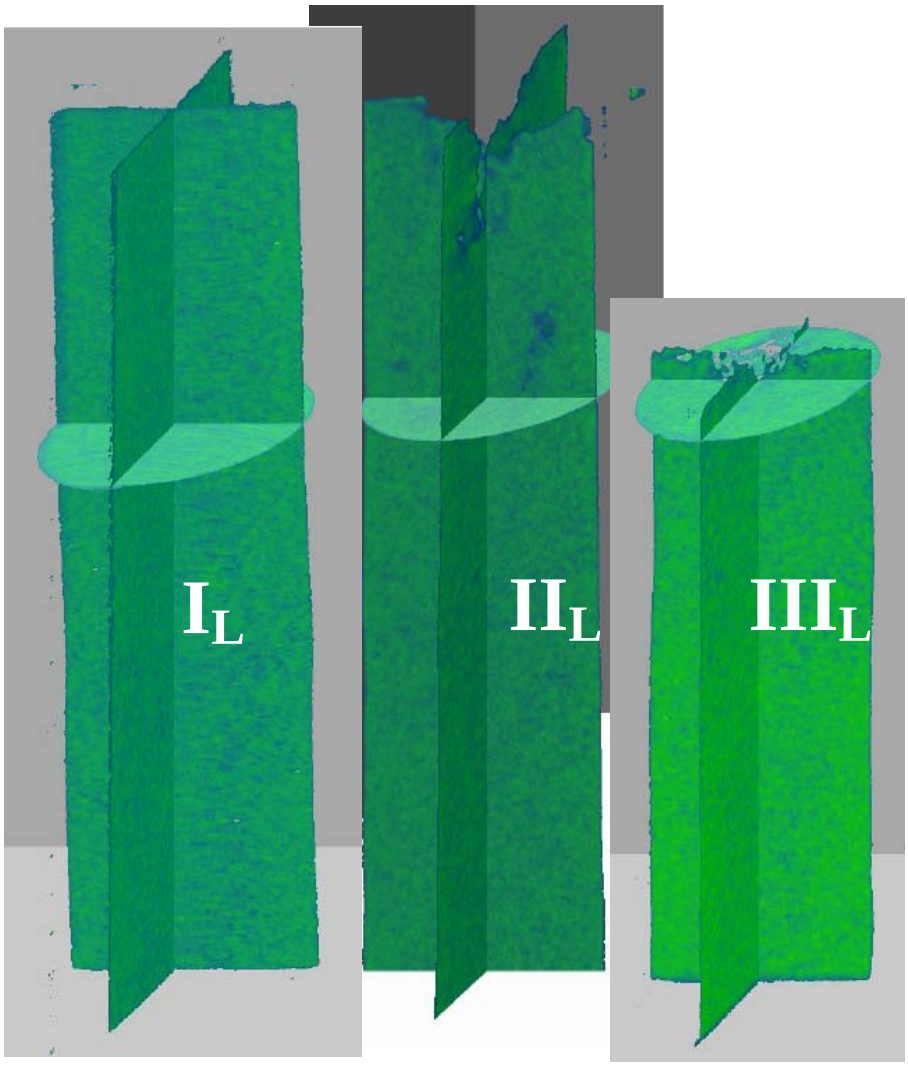

Figure 19. CT longitudinal sections of core after first flooding period with the Figure 18 corresponding cross sections marked (limestone Coreflood D).

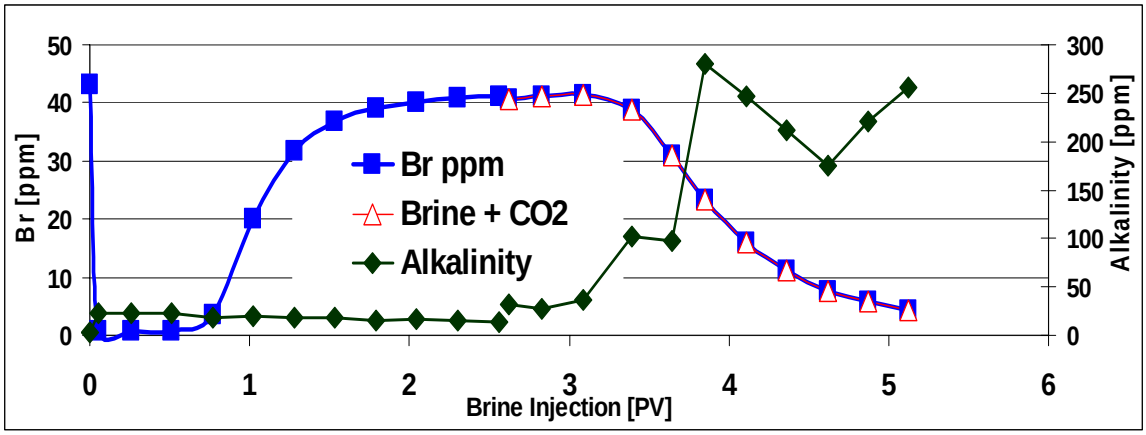

Figure 20. Bromide diffusivity and alkalinity results (limestone Coreflood D).

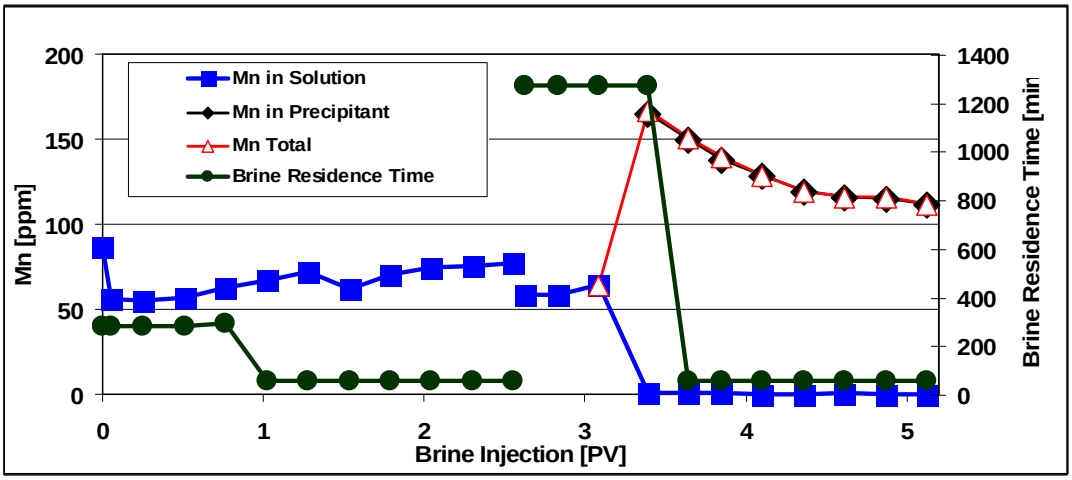

Figure 21. Manganese concentration in the effluent (limestone Coreflood D).

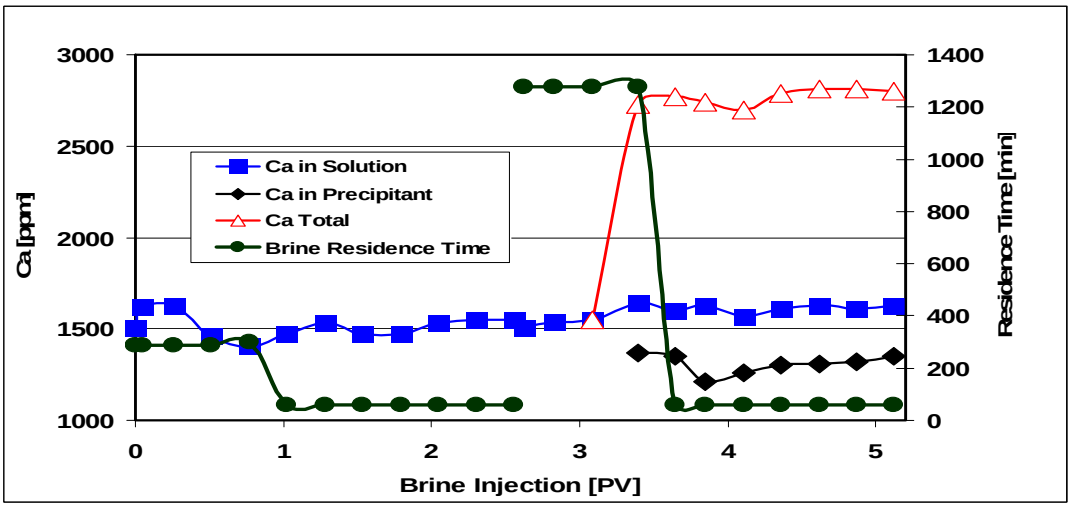

Figure 22. Calcium concentration in the effluent (limestone Coreflood D).

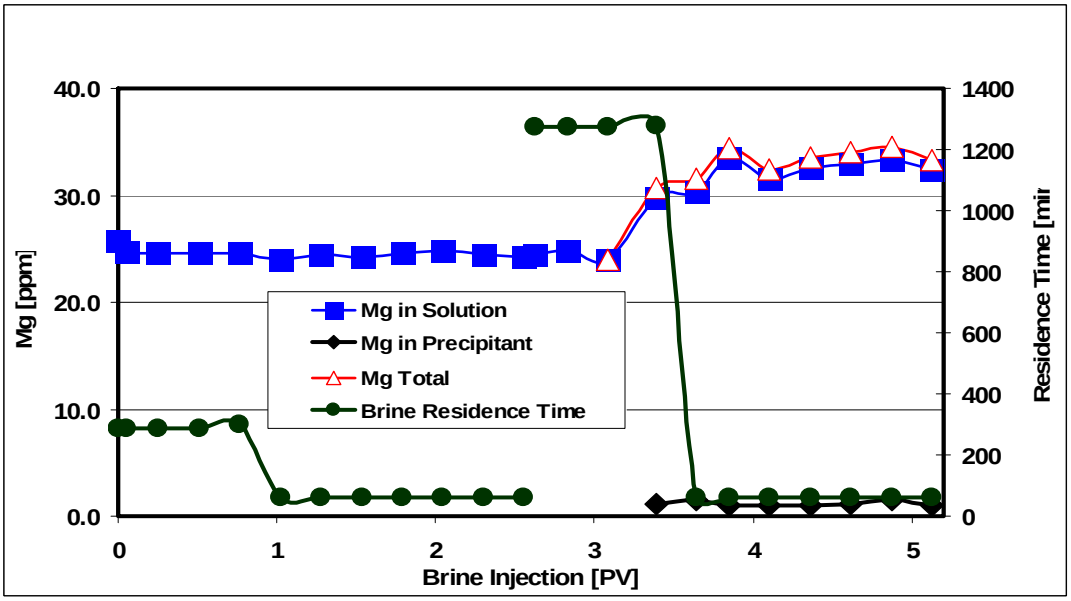

Figure 23. Magnesium concentration in the effluent (limestone Coreflood D).

Figure 24. Three dolomite core segments after the first flooding period (Coreflood E).

Figure 25. Inlet of first segment after each flooding period (dolomite Coreflood E).

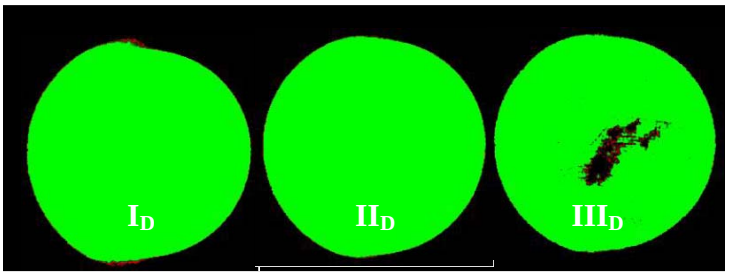

Figure 26. CT cross section images at ~6 cm from the end of the original dolomite Segment A inlet. Pre-flood (I_D), after the first flooding period (II_D), and post-flood (III_D) (Coreflood E).

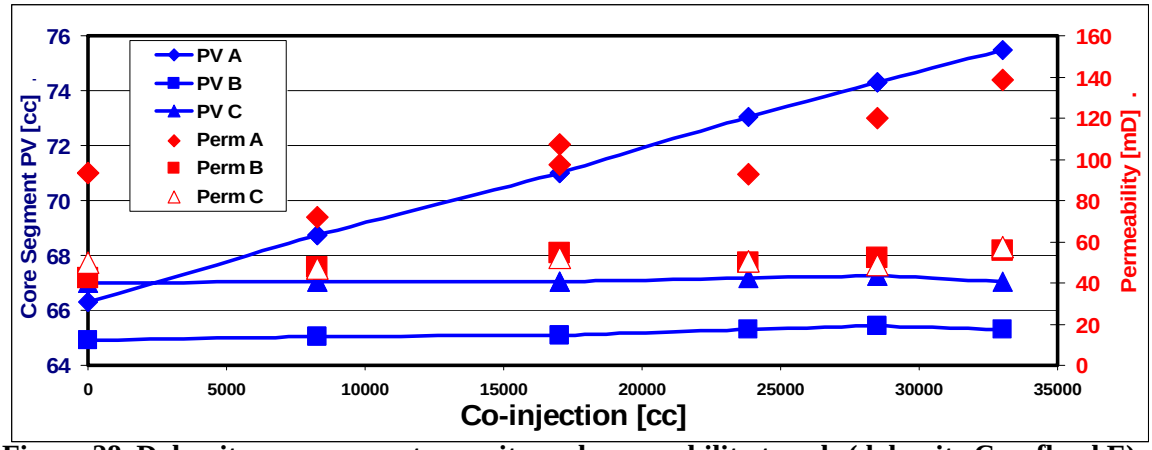

Figure 28. Dolomite core segment porosity and permeability trends (dolomite Coreflood E).

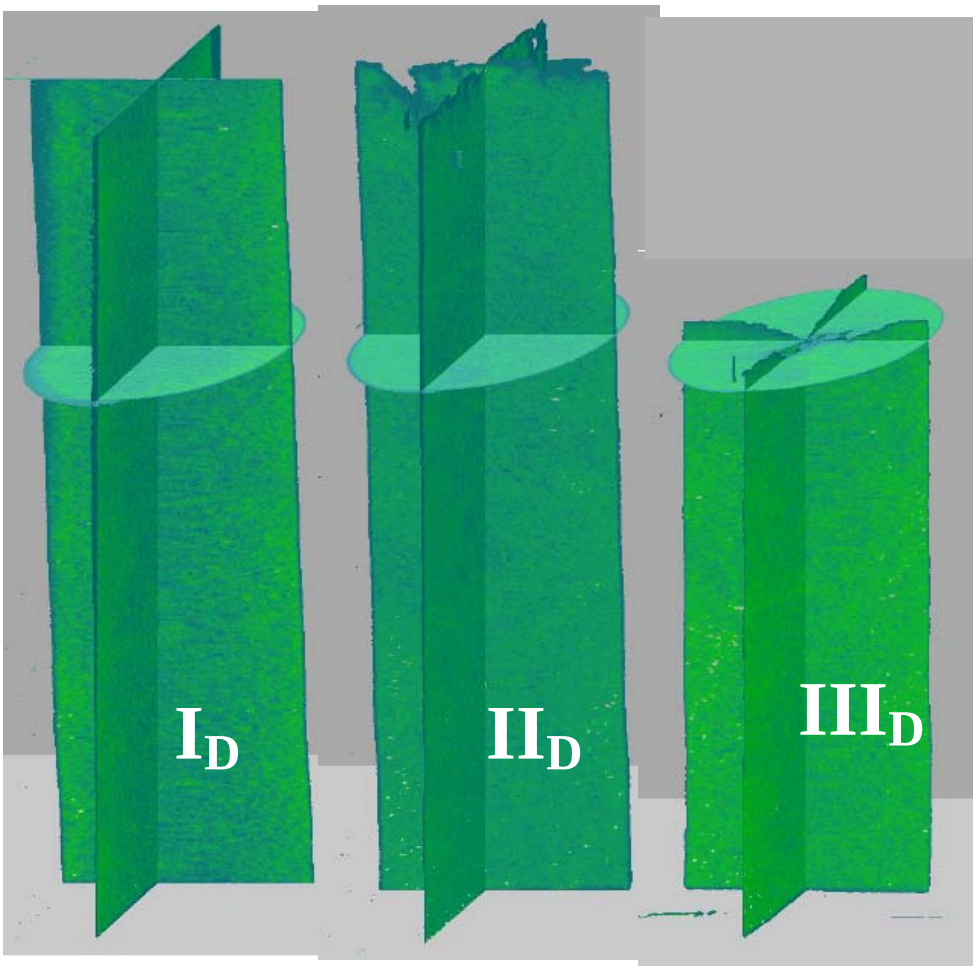

Figure 27. CT longitudinal sections of core after first flooding period with the Figure 26 corresponding cross section marked (dolomite Coreflood E).

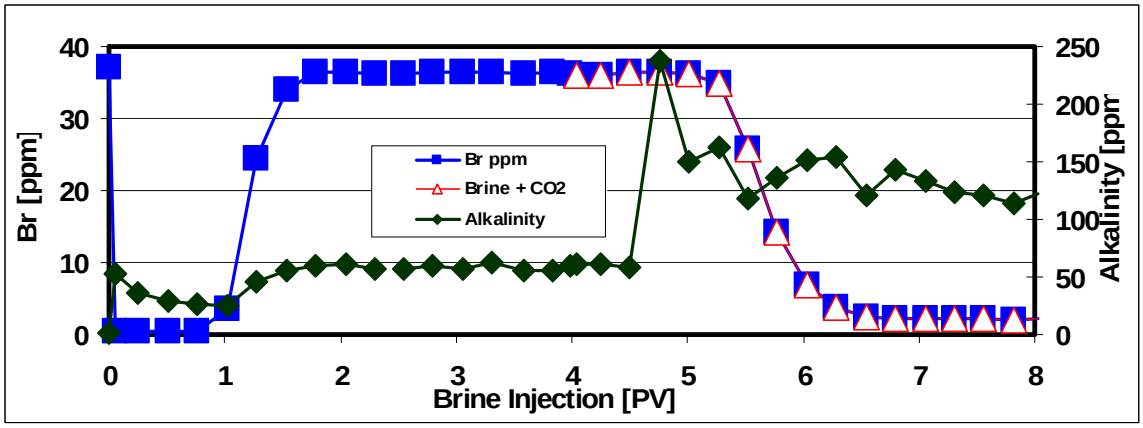

Figure 29. Bromide diffusivity and alkalinity results (dolomite Coreflood E).

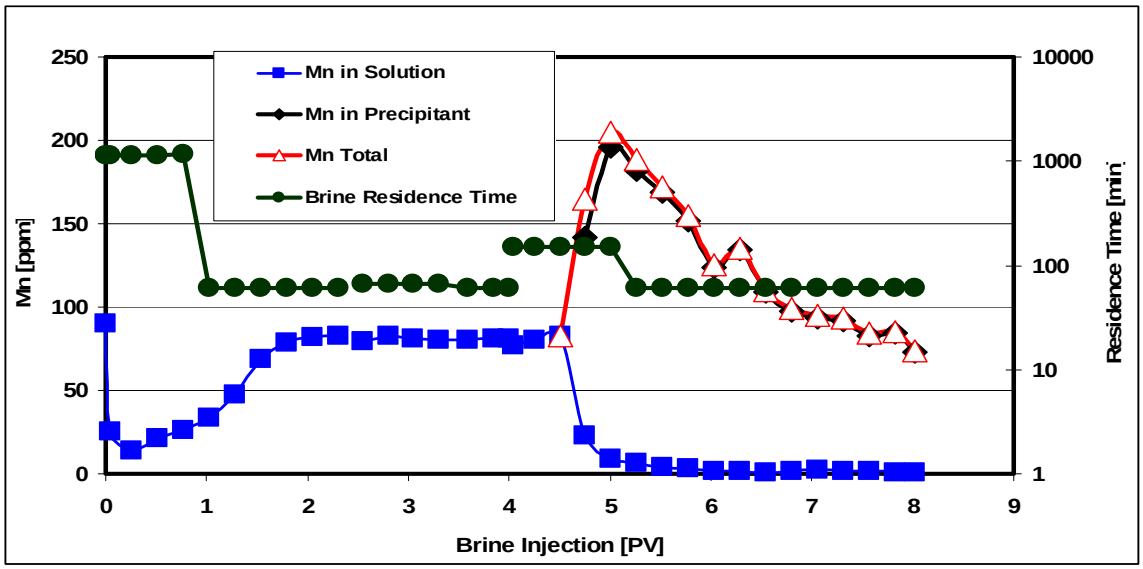

Figure 30. Manganese concentration in the effluent (dolomite Coreflood E).

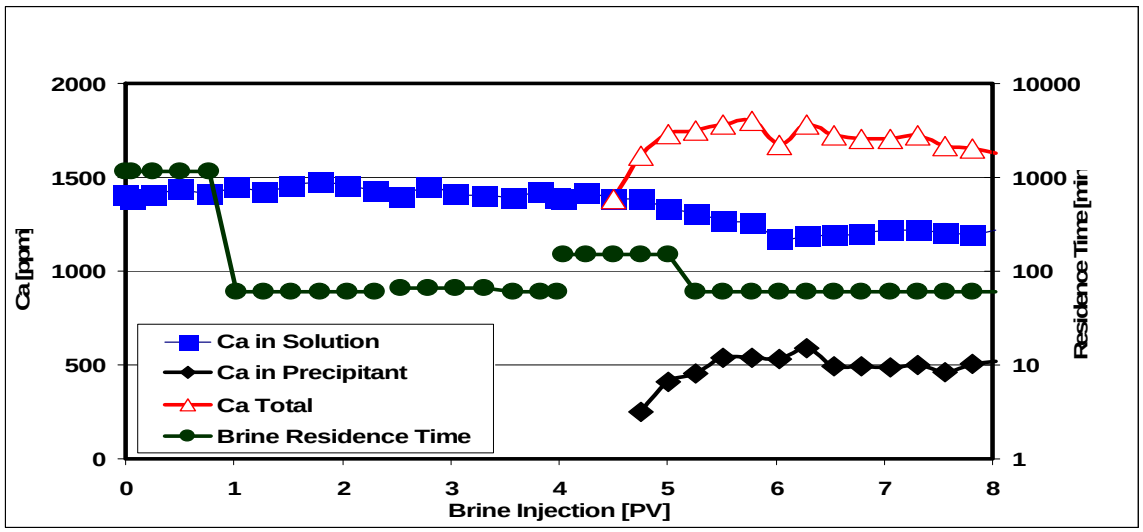

Figure 31. Calcium concentration in the effluent (dolomite Coreflood E).

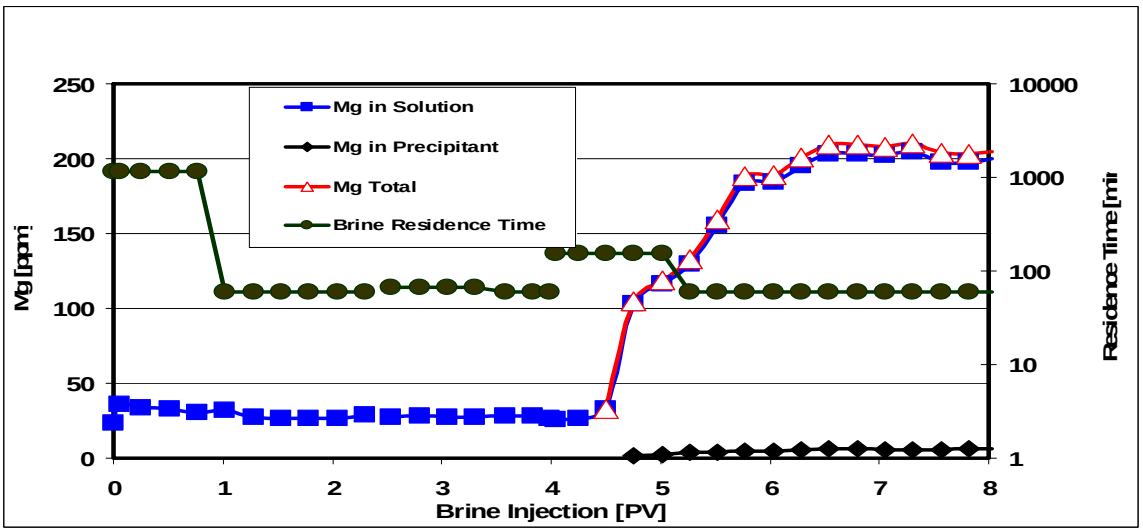

Figure 32. Magnesium concentration in the effluent (dolomite Coreflood E).